TTP16-018

χ_{c1} and χ_{c2} production at e^+e^- colliders. *

Henryk Czyż,[1] Johann H. Kühn,[2] and Szymon Tracz[1]

[1] *Institute of Physics, University of Silesia, PL-40007 Katowice, Poland.*
[2] *Institut für Theoretische Teilchenphysik, Karlsruhe Institute of Technology, D-76128 Karlsruhe, Germany.*

(Dated: May 24, 2016)

Direct, resonant production of the charmonium states χ_{c1} and χ_{c2} in electron-positron annihilation is investigated. Depending on details of the model, a sizeable variation of the prediction for the production cross section is anticipated. It is demonstrated that resonant production could be observed under favorable circumstances.

PACS numbers: 13.66.Bc, 13.40.Gp

I. INTRODUCTION

The exclusive production of narrow resonances in electron-positron annihilation has been up to now observed for states with the quantum numbers of the virtual photon, $J^{PC} = 1^{--}$, only. In principle axial vector resonances with $J^{PC} = 1^{++}$ can be produced directly through two distinctly different mechanisms: either electromagnetically through two virtual photons or through the neutral current. The tensor state with $J^{PC} = 2^{++}$, in contrast, can be produced through the electromagnetic process only. In practice, however, the rates are tiny at low energies and up to now only resonant production of hadrons with $J^{PC} = 1^{--}$ has been observed experimentally. Nevertheless, already quite early the production of 1^{++} and 2^{++} states has been suggested, either through the neutral current [1] or through two virtual photons [1, 2], with emphasis on charmonium resonances. In view of the small resonance enhancement, which is below or at most at the percent level, no experimental attempt has been made up to now to verify the predictions. However, with the advent of e^+e^- colliders with extremely high luminosity like BESIII, the picture has changed and this possibility has gained renewed interest [3–5]. It now seems that resonant production of χ_{c1} and χ_{c2} might eventually be accessible by experiments. The signal could be observed either in a resonant excess of the hadronic cross section $e^+e^- \to \chi_{cJ} \to$ hadrons or, alternatively, of the cross section $e^+e^- \to \chi_{cJ} \to J/\psi + \gamma$ with subsequent decay $J/\psi \to \mu^+\mu^-$. Note, that the interference with the continuum cross section $e^+e^- \to J/\psi + \gamma$, which is the result of obvious radiative corrections, might play an important role in this connection.

It is the purpose of this paper to investigate these possibilities in detail. We will first evaluate the resonant electromagnetic cross section both for the $J^{PC} = 1^{++}$ and the $J^{PC} = 2^{++}$ state, including the influence of interference with continuum reaction (Figure 1), recalling and extending earlier results [1–5]. Two different final states will be considered: the hadronic cross section from the resonant reaction $e^+e^- \to \chi_{cJ} \to$ hadrons, and the lepton plus photon state $e^+e^- \to \chi_{cJ} \to \gamma J/\psi(\to \mu^+\mu^-)$ together with its interference with the continuum $e^+e^- \to \gamma J/\psi(\to \mu^+\mu^-)$. Of course the e^+e^- energy has to be chosen equal to the mass of χ_{c_1} or χ_{c_2} and the photon energy has to be chosen in the proper kinematic region.

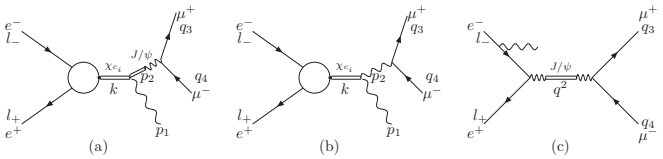

FIG. 1: Diagrams for the cross section for the process $e^+e^- \to \chi_{c_J} \to \gamma J/\psi(\to \mu^+\mu^-)$.

II. RESONANT χ_{c_J} PRODUCTION

A. Short distance approximation

Let us in a first step recall the results from [2, 5] on resonant χ_{c_J} production, using as a rough approximation the short distance expansion as discussed in [2]. The coupling to two virtual photons is given by

$$\begin{aligned} A_0^{\alpha\beta}(p_1,p_2)\epsilon^1_\alpha\epsilon^2_\beta \;=\; & \sqrt{\frac{1}{6}}c\frac{2}{M_{\chi_{c_0}}}\{[(\epsilon_1\epsilon_2)(p_1p_2) \\ & -(\epsilon_1p_2)(\epsilon_2p_1)][M^2_{\chi_{c_0}}+(p_1p_2)] \\ & +(\epsilon_1p_2)(\epsilon_2p_2)p_1^2+(\epsilon_1p_1)(\epsilon_2p_1)p_2^2 \\ & -(\epsilon_1\epsilon_2)p_1^2p_2^2-(\epsilon_1p_1)(\epsilon_2p_2)p_1p_2\}, \end{aligned} \tag{1}$$

$$\begin{aligned} A_1^{\alpha\beta}(p_1,p_2,\epsilon)\epsilon^1_\alpha\epsilon^2_\beta \;=\; & ic\{p_1^2(\epsilon,\epsilon_1,\epsilon_2,p_2)+p_2^2(\epsilon,\epsilon_2,\epsilon_1,p_1) \\ & +\epsilon_1p_1(\epsilon,\epsilon_2,p_1,p_2)+\epsilon_2p_2(\epsilon,\epsilon_1,p_2,p_1)\}, \end{aligned}$$

*Work supported in part by the Polish National Science Centre, grant number DEC-2012/07/B/ST2/03867 and German Research Foundation DFG under Contract No. Collaborative Research Center CRC-1044.

(2)

$$A_2^{\alpha\beta}(p_1,p_2,\epsilon)\epsilon^1_\alpha\epsilon^2_\beta = \sqrt{2}cM_{\chi_{c_2}}\{(p_1p_2)\epsilon^1_\mu\epsilon^2_\nu + p_{1\mu}p_{2\nu}(\epsilon_1\epsilon_2) - p_{1\mu}\epsilon^2_\nu(\epsilon_1p_2)) - p_{2\mu}\epsilon^1_\nu(\epsilon_2p_1))\}\epsilon^{\mu\nu}, \quad (3)$$

where

$$c \equiv c((p_1+p_2)^2,p_1^2,p_2^2,m) = \frac{16\pi\alpha a}{\sqrt{m}}\frac{1}{((p_1-p_2)^2/4-m^2+i\epsilon)^2}, \quad (4)$$

with m the effective charm quark mass in χ_{c_i}, $a = \sqrt{\frac{1}{4\pi}}3Q^2\phi'(0)$, $\phi'(0)$ the derivative of the wave function at the origin and $Q = 2/3$ the charm quark electric charge. p_1^2, p_2^2, ϵ_1, ϵ_2 are the squares of the momenta and the polarization vectors of the photons and ϵ is the polarization vector in case of χ_{c_1} and the polarization tensor in case of χ_{c_2}. We have checked that terms in the amplitudes, which are proportional to the binding energies and neglected in [2], are breaking gauge invariance. Thus the results, Eqs.(1-3), do contain all the allowed binding energy corrections. Using this form of the photon resonance coupling, the amplitude for electron-positron annihilation is given by a loop integral and can be cast into the form:

$$A(e^+e^- \to^3 P_J) = ie^2\int\frac{dp_1}{(2\pi)^4}\bar{v}(l_+)\gamma_\nu\,\not{h}\gamma_\mu u(l_-)\frac{1}{h^2}\frac{1}{p_1^2}\frac{1}{p_2^2}A_J^{\mu\nu}(p_1,p_2,\epsilon), \quad (5)$$

with $h = l_- - p_1$. Since we neglect the electron mass throughout, the amplitudes are given by

$$A(e^+e^- \to^3 P_0) = 0, \quad (6)$$

$$A(e^+e^- \to^3 P_1) = g_1\bar{v}\gamma_5\not{\epsilon}u, \quad (7)$$

$$A(e^+e^- \to^3 P_2) = g_2\bar{v}\gamma^\mu u\epsilon_{\mu\nu}(l_+^\nu - l_-^\nu)/M_{\chi_{c_2}}. \quad (8)$$

As shown in [5] the mass corrections are completely negligible for electrons. For the coefficients characterizing the amplitudes one finds [2]

$$g_1 = -\frac{\alpha^2\sqrt{2}}{M_{\chi_{c_1}}^{5/2}}32a\log\frac{2b_1}{M_{\chi_{c_1}}}, \quad (9)$$

$$g_2 = \frac{\alpha^2}{M_{\chi_{c_2}}^{5/2}}64a[\log\frac{2b_2}{M_{\chi_{c_2}}} + \frac{1}{3}(i\pi+\log 2-1)], \quad (10)$$

with binding energy defined as $b_i = 2m - M_{\chi_{c_i}}$. Notice that the definition of a in [2] is different by a factor $\sqrt{3m}Q^2$ from the definition used here. The electronic widths are given by

$$\Gamma(^3P_1 \to e^+e^-) = \frac{1}{3}\frac{|g_1|^2}{4\pi}M_{\chi_{c_1}}, \quad (11)$$

$$\Gamma(^3P_2 \to e^+e^-) = \frac{1}{5}\frac{|g_2|^2}{8\pi}M_{\chi_{c_2}}. \quad (12)$$

Note that the result for $J = 2$ differs from the one of [2] by a factor 2. Furthermore the factor $3Q_i^4$ has been taken into account in the definition of a. The numerical results are expected to depend significantly on the precise value of the charmed quark mass and the relative size of the absorptive part. For negative value of b the amplitudes develops a sizeable absorptive part which subsequently simulates the contribution from the intermediate state $J/\psi+\gamma$.

B. Binding energy corrections

In the next step we include binding energy corrections into the result. We thus include terms of order $1-x$ with $x = \frac{4m^2}{M^2_{\chi_{c_i}}}$. The decay rates are now given by:

$$\Gamma(\chi_{c_1} \to e^+e^-) = \frac{1}{3}\frac{|g_{1_{\gamma\gamma}}|^2}{4\pi}M_{\chi_{c_1}}, \quad (13)$$

$$\Gamma(\chi_{c_2} \to e^+e^-) = \frac{1}{5}\frac{|g_{2\gamma\gamma}|^2}{8\pi}M_{\chi_{c_2}}. \quad (14)$$

with the coupling $g_{1_{\gamma\gamma}}$ and $g_{2_{\gamma\gamma}}$ given by

$$g_{1_{\gamma\gamma}} = \frac{16\alpha^2 a}{\sqrt{m}M^2_{\chi_{c_1}}}\left[\log\left(\frac{x}{1+x}\right)(1-x) - \left(\log\left(\frac{x}{1-x}\right)+i\pi\right)(1+x)\right], \quad (15)$$

$$g_{2_{\gamma\gamma}} = \frac{32\sqrt{2}\alpha^2 a}{3\sqrt{m}M^2_{\chi_{c_2}}}\left[\left(\frac{1+x}{2}+\frac{8}{(1+x)^2}\right)\log(1-x) + \frac{3}{2}(1+x)\log(1+x) - 2\left(1+x+\frac{2}{(1+x)^2}\right)\log(x) - \frac{8}{(1+x)^2}\log(2) - 1 - \frac{i\pi}{2}\left(1+x+\frac{8}{(1+x)^2}\right)\right]. \quad (16)$$

Of course, in the limit $x \to 1$ the results from equations (9) and (10) are recovered. Leading order approximation and exact results for positive and negative binding energy are given in Table I, where we have used a typical value of $0.1GeV^5$ for $|\phi^{`}(0)|^2$.

C. Short and Long distance combined

Although the model discussed in the previous section exhibits the correct leading logarithmic behavior of the photon-photon -χ_{c_i} coupling, the non-enhanced terms

	$\Gamma(\chi_{c_1} \to e^+e^-)$	$\Gamma(\chi_{c_2} \to e^+e^-)$
	$b = 0.5\ GeV$	
Leading term	0.0226 eV	0.0243 eV
exact result	0.0317 eV	0.0159 eV
	$b = -0.5\ GeV$	
Leading term	0.164 eV	0.0512 eV
exact result	0.141 eV	0.0731 eV

TABLE I: Electronic widths for $b = -0.5GeV$ and $b = 0.5GeV$

are of comparable size, potentially even larger than the formally dominant ones. For this reason we formulate an ansatz which gives the correct behavior for the coupling of χ_{c2} to two photons and for the coupling of both χ_{c_1} and χ_{c_2} to $J/\psi\gamma$. We start from the following ansatz (see Figs. 2, 3):

$$A^{\alpha\beta}_{1\gamma\gamma}(p_1,p_2,\epsilon)\epsilon^1_\alpha\epsilon^2_\beta\Big|_{p_1^2=p_2^2=0} = 0, \tag{17}$$

$$A^{\alpha\beta}_{1\gamma J/\psi}(p_1,p_2,\epsilon)\epsilon^1_\alpha\epsilon^2_\beta\Big|_{p_1^2=0,\ p_2^2=M^2_{J/\psi}} = ic^1_{J/\psi}\Big\{p_2^2(\epsilon,\epsilon_2,\epsilon_1,p_1) + \epsilon_1 p_1(\epsilon,\epsilon_2,p_1,p_2) + \epsilon_2 p_2(\epsilon,\epsilon_1,p_2,p_1)\Big\}, \tag{18}$$

$$A^{\alpha\beta}_{2\gamma\gamma}(p_1,p_2,\epsilon)\epsilon^1_\alpha\epsilon^2_\beta\Big|_{p_1^2=p_2^2=0} = \sqrt{2}c^2_\gamma M_{\chi_{c_2}}\Big\{(p_1p_2)\epsilon^1_\mu\epsilon^2_\nu + p_{1\mu}p_{2\nu}(\epsilon_1\epsilon_2) - p_{1\mu}\epsilon^2_\nu(\epsilon_1p_2)) - p_{2\mu}\epsilon^1_\nu(\epsilon_2p_1))\Big\}\epsilon^{\mu\nu}, \tag{19}$$

$$A^{\alpha\beta}_{2\gamma J/\psi}(p_1,p_2,\epsilon)\epsilon^1_\alpha\epsilon^2_\beta\Big|_{p_1^2=0,\ p_2^2=M^2_{J/\psi}} = \sqrt{2}c^2_{J/\psi}M_{\chi_{c_2}}\Big\{(p_1p_2)\epsilon^1_\mu\epsilon^2_\nu + p_{1\mu}p_{2\nu}(\epsilon_1\epsilon_2) - p_{1\mu}\epsilon^2_\nu(\epsilon_1p_2)) - p_{2\mu}\epsilon^1_\nu(\epsilon_2p_1))\Big\}\epsilon^{\mu\nu}, \tag{20}$$

where, in the case of the amplitudes $A_{i\gamma\gamma}$, p_1 and p_2 are the momenta of photons, ϵ_1 and ϵ_2 are their polarization vectors. In the case of the amplitudes $A_{i\gamma J/\psi}$, p_1 is the photon momentum, ϵ_1 its polarization vector, p_2 is the J/ψ momentum and ϵ_2 its polarization vector. The function c_γ is the $\chi_{c_i} - \gamma\gamma$ form factor, whereas $c_{J/\psi}$ is the $\chi_{c_i} - \gamma J/\psi$ form factor. These form factors have the following forms:

$$c^i_\gamma \equiv (1 + \frac{f\cdot a_J}{aM^2_{J/\psi}})c(M^2_{\chi_{c_i}},0,0,m) =$$

$$c_\gamma = \frac{4e^2}{\sqrt{m}}(a + \frac{fa_J}{M^2_{J/\psi}})\frac{1}{(M^2_\chi/2+b^2/4+bM_\chi/2)^2}$$

FIG. 2: Diagrams for decay widths $\Gamma(\chi_{c_{0,1,2}} \to \gamma\gamma)$.

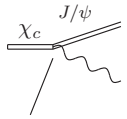

$$c_{J/\psi} = \frac{4ea_J}{\sqrt{m}}\frac{1}{(M^2_\chi/2+b^2/4+bM_\chi/2-M^2_{J/\psi}/2)^2}$$

FIG. 3: Diagrams for decay widths $\Gamma(\chi_{c_{0,1,2}} \to \gamma J/\psi)$.

$$\frac{16\pi\alpha}{\sqrt{m}}(a + \frac{fa_J}{M^2_{J/\psi}}) \frac{1}{\Big(M^2_{\chi_{c_i}}/2 + b_i^2/4 + b_iM_{\chi_{c_i}}/2\Big)^2}, \tag{21}$$

$$c^i_{J/\psi} \equiv \frac{a_J}{ae}c(M^2_{\chi_{c_i}},0,M^2_{J/\psi},m) = \frac{4ea_J}{\sqrt{m}}\frac{1}{\Big(M^2_{\chi_{c_i}}/2 + b_i^2/4 + b_iM_{\chi_{c_i}}/2 - M^2_{J/\psi}/2\Big)^2}. \tag{22}$$

The coupling a_J in our model is a free parameter. With this ansatz one obtains

$$\Gamma(\chi_{c_1} \to J/\Psi\gamma) = \frac{1}{96\pi}|c^1_{J/\psi}|^2M^2_{J/\Psi}M^3_{\chi_{c_1}}(1+x_1)(1-x_1)^3, \tag{23}$$

$$\Gamma(\chi_{c_2} \to \gamma\gamma) = \frac{1}{160\pi}|c^2_\gamma|^2M^5_{\chi_{c_2}}, \tag{24}$$

$$\Gamma(\chi_{c_2} \to J/\Psi\gamma) = \frac{1}{80\pi}|c^2_{J/\psi}|^2M^5_{\chi_{c_2}}(1-x_2)^3(1+x_2/2+x_2^2/6), \tag{25}$$

where $x_i = M^2_{J/\Psi}/M^2_{\chi_{c_i}}$ and c^i_γ, $c^i_{J/\psi}$ are defined in Eq. (21) and (22). The parameter a has been defined after Eq.(4). The constant f has been extracted from the electronic width of J/ψ calculated according to the diagram from Fig. 4 and has the following form:

$$f = \sqrt{\frac{3\Gamma_{J/\psi\to e^+e^-}M^3_{J/\psi}}{4\pi\alpha^2}}. \tag{26}$$

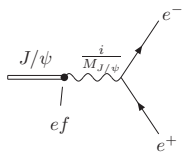

FIG. 4: Diagram for decay width $\Gamma(J/\psi \to e^+e^-)$.

The R_{peak} value at the peak of the cross section is given by [6]

$$R_{peak} = \frac{\sigma^{(0)}_{res}}{\sigma_{pt}} = \frac{\Gamma_{ee}}{\Delta}\frac{9}{4\alpha^2}\sqrt{2M}\frac{\Gamma_{had}}{\Gamma_{tot}}N_Z \qquad (27)$$

where $\Gamma_{ee}, \Gamma_{had}$ and Γ_{tot} denote the width of the resonance into e^+e^-, into hadrons and the total width, respectively. Δ stands for the machine energy resolution and N_Z is slightly model dependent factor around 0.7. Taking for illustration values for Γ_{ee} between 0.1 eV and 0.5 eV, $\Gamma_{had}/\Gamma_{tot} = 0.66$ and $\Delta = 4MeV$, one finds R_{peak} between $2.15{\cdot}10^{-3}$ and $1.075{\cdot}10^{-2}$.

Alternatively, one may focus on the decay channel $e^+e^- \to \chi_{c_i} \to \gamma J/\psi(\to \mu^+\mu^-)$. For the 1^{++} state the prediction is also affected by the amplitude due to the neutral current [1, 2, 5] . To identify the interference term, the neutral current amplitude has to be decomposed into the form $(V_e+A_e)A_C$, and it is the interference between the A_eA_C term from the neutral current and the dispersive part (real part) of the electromagnetic amplitude which affects the rate. Specifically one obtains:

$$\Gamma(\chi_{c_1} \to e^+e^-) = \frac{M_{\chi_{c_1}}}{3\pi}\left[\frac{|g_1|^2}{4} + \frac{aG_F}{\sqrt{2m}Q^2}Re(g1) + \frac{a^2G_F^2}{mQ^4}\left(1 - 4\sin^2\theta_W + 8\sin^4\theta_W\right)\right], \qquad (28)$$

where G_F is the Fermi constant and θ_W is the weak mixing angle. The function g_1 comes from performing loop integrals (see Appendix A).
The mass of the c quark, the derivative of the wave function at the origin (in fact a) and the parameter a_J have been extracted from the measured decay widths [7] of $\chi_{c1,2}$ to $\gamma\gamma$ and to $\gamma J/\psi$, using formulae (23), (24), (25). The obtained parameters, the square of the derivative of the wave function $|\phi^{'}(0)|^2$, the binding energies calculated according to $b_i = 2m - M_i$, and the parameter a_J are presented in Table II together with the calculated decay widths.

The electronic widths have been calculated using the diagrams from Figure 5. For χ_{c_1} we have, in addition, also included the contribution coming from the neutral current Eq. (29). The functions g_i, which come from

a[GeV$^{5/2}$]	$\lvert\phi^{'}(0)\rvert^2$ [GeV^5]	m [GeV]	b_1 [GeV]	b_2[GeV]	a_J
0.073	0.04	1.7	-0.204	-0.249	0.11

widths [MeV]	χ_{c1}	χ_{c2}
$\Gamma(\chi \to \gamma\gamma)_{th}$	-	$5.28819 \cdot 10^{-4}$
$\Gamma(\chi \to J/\psi\gamma)_{th}$	$2.84760 \cdot 10^{-1}$	$3.70560 \cdot 10^{-1}$
$\Gamma(\chi \to \gamma\gamma)_{exp}$	-	$5.3(3) \cdot 10^{-4}$
$\Gamma(\chi \to J/\psi\gamma)_{exp}$	$2.8(2) \cdot 10^{-1}$	$3.7(3) \cdot 10^{-1}$

TABLE II: Parameters and theoretical (th) (this paper), and experimental (exp) [7] values of $\Gamma(\chi_{1,2} \to \gamma\gamma, \gamma J/\psi)$.

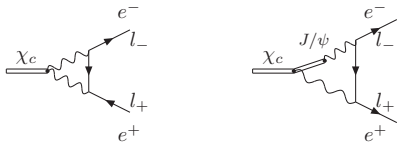

FIG. 5: Diagrams for decay widths $\Gamma(\chi_{c_{0,1,2}} \to e^+e^-)$.

performing loop integrals can be divided into two parts:

$$g_i = g_{i_{\gamma\gamma}} + g_{i_{J/\psi\gamma}}, \qquad (29)$$

coming from Fig.5a and Fig.5b. The formulae for these functions can be found in Appendix A. In Table III we present the values of the electronic widths within the adopted model, where $g_{i_{\gamma\gamma}}$ is the contribution from the diagram with two photons, $g_{i_{J/\psi\gamma}}$ the contribution from the diagram which contains $J/\psi\gamma$. For χ_{c_1} we include the sum of electromagnetic and neutral current contribution ($QED + Z^0$). The obtained values of the electronic widths are quite comparable to the ones obtained within other models [2–5].

III. THE PROCESS $e^+e^- \to \chi_{c_i} \to \gamma J/\psi(\to \mu^+\mu^-)$

With the couplings extracted as described above one can predict the χ_{c_1} and χ_{c_2} production cross sections in e^+e^- annihilation. As these states are not stable one can observe only their decay products and an easy to identify final state has to be chosen. An obvious choice is the reaction $e^+e^- \to \chi_c \to \gamma J/\psi(\to \mu^+\mu^-)$. The Feynman diagram describing this process is given in Fig.1a. In Fig.1b we present the diagram for the similar process,

	$\gamma\gamma + J/\psi\gamma$	$\gamma\gamma$	$J/\psi\gamma$	QED+Z^0
$\Gamma(\chi_{c_1} \to e^+e^-)$ [eV]	0.078	0.073	0.003	0.071
$\Gamma(\chi_{c_2} \to e^+e^-)$ [eV]	1.35	0.032	0.975	-

TABLE III: Electronic widths for χ_{c_1} and χ_{c_2}. See text for details

where J/ψ is substituted by γ. The same final state is produced also in the ISR process (Fig. 1c) and the two amplitudes interfere.

Within the adopted model the χ_{ci} production amplitudes read

$$\mathcal{M}_0 = 0, \tag{30}$$

$$\begin{aligned}\mathcal{M}_1 = & \Big\{ g_1 \bar{v}(l_+)\gamma_5\gamma^\mu u(l_-) \\ & + \frac{2aG_F M^2_{\chi_{c_1}}}{f}\bar{v}(l_+)\Big((1+2m/M_{\chi_{c_1}})\gamma_5\gamma^\mu \\ & + (1-4\sin^2\theta_W + 2m/M_{\chi_{c_1}} \\ & - 8m/M_{\chi_{c_1}}\sin^2\theta_W)\gamma^\mu\Big)u(l_-)\Big\} \\ & \Pi^{\chi_{c1}}_{\mu\nu}(k)\ A_1^{\nu\beta}\ \Pi^{J/\psi}_{\beta\delta}(p_2)\ e\ \bar{u}(q_3)\gamma^\delta v(q_4)\end{aligned} \tag{31}$$

$$\begin{aligned}\mathcal{M}_2 = & \ g_2\bar{v}(l_+)\gamma^\mu u(l_-)(l_+^\nu - l_-^\nu)/M_{\chi_{c_2}} \\ & \Pi^{\chi_{c2}}_{\mu\nu\alpha\beta}(k)\ A_2^{\alpha\beta\gamma}\ \Pi^{J/\psi}_{\gamma\delta}(p_2)\ e\ \bar{u}(q_3)\gamma^\delta v(q_4),\end{aligned} \tag{32}$$

where $f = 2\sqrt{2}(M_{\chi_{c_1}}/2+m)M_{\chi_{c_1}}\sqrt{m}Q^2$. The amplitudes $A_i^{\nu\beta}$ can be found in Appendix B of [2],

$$A_1^{\nu\beta} = -i\frac{1}{2}c(I_1^{1\,\nu\beta} + I_2^{1\,\nu\beta}), \tag{33}$$

$$A_2^{\alpha\beta\gamma} = -c\sqrt{2}M_{\chi_{c_2}} I_2^{2\alpha\beta\gamma}, \tag{34}$$

and coincide with Eq.(2) and Eq.(3) Here the contributions I_1^1, I_2^1 and I_2^2 are given by:

$$I_1^{1\,\nu\beta} = \epsilon^{\bar{\mu}\bar{\nu}\beta\nu}F^1_{\bar{\mu}\bar{\nu}}p^2_{\bar{\gamma}}p^{2\bar{\gamma}} - \epsilon^{\bar{\mu}\bar{\nu}\bar{\alpha}\nu}F^1_{\bar{\mu}\bar{\nu}}p^2_{\bar{\alpha}}p^{2\beta}, \tag{35}$$

$$I_2^{1\,\nu\beta} = 0, \tag{36}$$

$$I_2^{2\alpha\beta\gamma} = F^{1\alpha\delta}\left(g^{\beta\gamma}p^2_\delta - g^\gamma_\delta p^{2\beta}\right), \tag{37}$$

where

$$F^1_{\mu\nu} = \epsilon^1_\mu p^1_\nu - \epsilon^1_\nu p^1_\mu. \tag{38}$$

The $I_2^{1\,\nu\beta}$ vanishes for one real photon in the vertex. The coupling of J/ψ to muons and the J/ψ propagator collected in $\Pi^{J/\psi}$, are given by,

$$\Pi^{J/\psi}_{\beta\delta}(p) = \sqrt{\frac{3\Gamma_{J/\psi\to e^+e^-}}{\alpha\sqrt{p_2^2}}}\frac{g_{\beta\delta} - p_\beta p_\delta/M^2_{J/\psi}}{p_2^2 - M^2_{J/\psi} + iM_{J/\psi}\Gamma_{J/\psi}}, \tag{39}$$

while the χ_{c1} propagator $\Pi^{\chi_{c1}}$ has the following form:

$$\Pi^{\chi_{c1}}_{\mu\nu}(k) = \frac{g_{\mu\nu} - k_\beta k_\delta/M^2_{\chi c1}}{k^2 - M^2_{\chi_{c_1}} + i\Gamma_{\chi_{c_1}}M_{\chi_{c_1}}}, \tag{40}$$

where k is the four-momentum of the χ_{c_1}, $M_{\chi_{c_1}}$ and $\Gamma_{\chi_{c_1}}$ are its mass and its decay width respectively. The χ_{c_2} propagator $\Pi^{\chi_{c2}}$ has the following form:

$$\Pi^{\chi_{c2}}_{\mu\nu\alpha\beta}(k) = \frac{B_{\mu\nu\alpha\beta}}{k^2 - M^2_{\chi_{c_2}} + i\Gamma_{\chi_{c_2}}M_{\chi_{c_2}}}, \tag{41}$$

where we use similar notation as for χ_{c_1}. The tensor $B_{\mu\nu\alpha\beta}$ is given by the following formula:

$$B_{\mu\nu\alpha\beta} = \frac{1}{2}(P_{\mu\alpha}P_{\nu\beta} + P_{\mu\beta}P_{\nu\alpha}) - \frac{1}{3}P_{\mu\nu}P_{\alpha\beta}), \tag{42}$$

where $P_{\mu\nu} = -g_{\mu\nu} + k_\mu k_\nu/M_{\chi_{c_2}}$. The form factor c is given in Eq.(4).

IV. IMPLEMENTATION INTO THE PHOKHARA GENERATOR: TESTS AND RESULTS

The amplitudes described in the previous section were implemented into the PHOKHARA event generator and will appear at the web page *(http://ific.uv.es/∼rodrigo/phokhara/)* as release 9.2. The radiative return amplitude was already implemented in the version 7.0 [8, 9]. The implementation of the other amplitudes was tested by constructing two independent codes: one using a trace method to sum over polarizations of initial and final particles, the second one using the helicity amplitude method with a basis chosen as in [10]. Excellent agreement of relative accuracy about 10^{-15}, was found except in the region where the amplitudes have zeros, but even for these negligible contributions several digits of the results agree.

Another test consisted of a comparison of the integrated cross section obtained by the PHOKHARA generator and an analytic form ($\sigma_{1,2}$) obtained with the amplitude from figure 1a for the scattering energy $\sqrt{s} = M_{\chi_{c_{1,2}}}$ in the narrow width approximation given below

$$\begin{aligned}\sigma_1 = & \frac{12\pi}{s}Br(\chi_{c_1}\to e^+e^-) \\ & Br(\chi_{c_1}\to J/\psi\gamma)Br(J/\psi\to\mu^+\mu^-),\end{aligned} \tag{43}$$

$$\begin{aligned}\sigma_2 = & \frac{20\pi}{s}Br(\chi_{c_2}\to e^+e^-) \\ & Br(\chi_{c_2}\to J/\psi\gamma)Br(J/\psi\to\mu^+\mu^-),\end{aligned} \tag{44}$$

with the partial widths given in Eqs.(23,25,11,12) and

$$\begin{aligned}&\Gamma_{J/\psi\to\mu^+\mu^-} = \\ &(1+2\frac{m_\mu^2}{M^2_{J/\psi}})\sqrt{1-4m_\mu^2/M^2_{J/\psi}}.\ \Gamma_{J/\psi\to e^+e^-}.\end{aligned} \tag{45}$$

The total widths are taken from [7]. As all the widths here are narrow, the approximation works well. The relative difference between the generator results and the analytic formulae Eq.(44) are $(0.49\pm0.07)\%$ for χ_{c_1} and $(2.81\pm0.02)\%$ for χ_{c_2}.

The predicted values of the electronic widths are rather small. More optimistic values, up to a factor 10 bigger, can be obtained within the vector dominance model of [2]. Yet, even with these relatively small values one can potentially observe the signal over the radiative return background. In Figures 6 and 8 we show the cross sections of the reactions $e^+e^-\to\mu^+\mu^-\gamma$ imposing angular

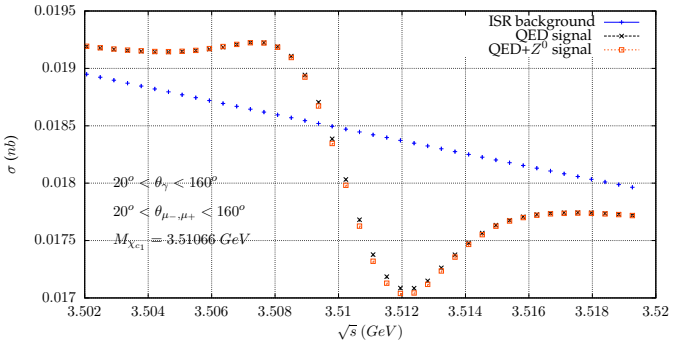

FIG. 6: The cross section $e^+e^- \to \mu^+\mu^-\gamma$, see text for details.

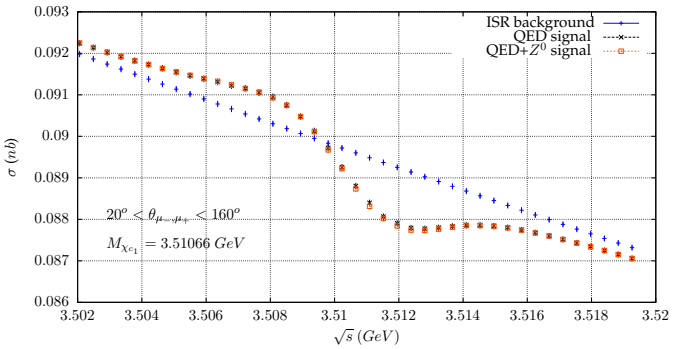

FIG. 7: The cross section $e^+e^- \to \mu^+\mu^-\gamma$, see text for details.

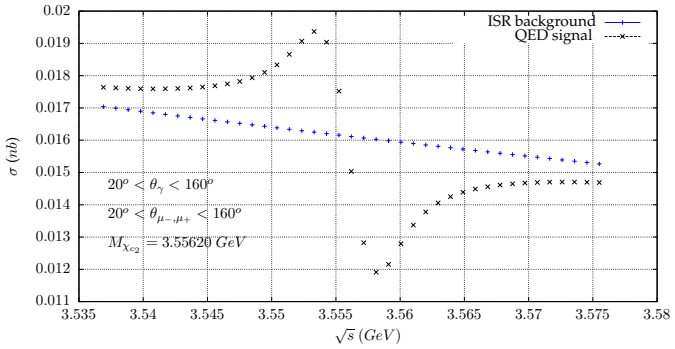

FIG. 8: The cross section $e^+e^- \to \mu^+\mu^-\gamma$, see text for details.

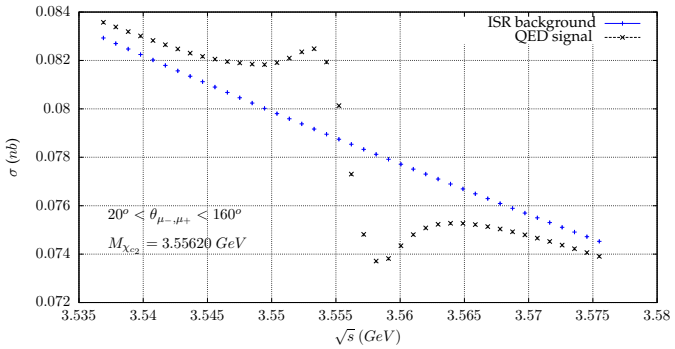

FIG. 9: The cross section $e^+e^- \to \mu^+\mu^-\gamma$, see text for details.

cuts on photons, whereas in Figures 7 and 9 we present these cross sections without imposing this cuts. In both cases we have assumed the χ_{c_1} and χ_{c_2} electronic widths as listed in Table III. A beam spread of 1 MeV per beam with Gaussian distribution was assumed. A possible contribution from the diagram in Fig. 1(b) is negligible for event selections used in the plots, where the muon pair invariant mass was chosen to be within 3 J/ψ widths within J/ψ mass (detector resolution was not taken into account). In the distributed version of the generator the diagram with $\chi_{c_i} \to \gamma^*(\to \mu^+\mu^-)\gamma$ is included. As the contribution of Z^0 to the χ_{c_i} width is tiny, the same is expected for the diagram similar to Fig.1(c) with γ substituted with Z^0 and these contributions were neglected.

A signal of up to 10 % of the radiative return background can be observed. The cross section is obviously bigger, when the photon is not tagged, but the signal to background ratio is smaller. Hopefully the BES-III collaboration will be able to measure these cross sections and extract the electronic widths of the χ_{c_1} and χ_{c_2}. The scan in the vicinity of these two charm states would also provide the possibility of testing the models and extracting the phase between the radiative return and the χ_{c_1} (χ_{c_2}) production amplitudes. As one can observe, with the relative phases between the amplitudes predicted within the model adopted in this paper, the production of χ_{c_1} and χ_{c_2} can be mainly observed as an interference between the ISR and the signal diagrams.

V. CONCLUSIONS

Diract, resonant production of χ_{c1} and χ_{c2} in electron-positron annihilation through two virtual photons will lead to a small, but nevertheless measurable resonant enhancement of the cross section. The prediction exhibits a sizeable model dependence, a consequence of the fact that predictions for charmonium, based on the nonrelativistic potential model are of qualitative nature only. Nevertheless, a resonant signal both in the hadronic cross section and in the $\gamma\mu^+\mu^-$ channel could be seen at the BESIII storage ring under favorable circumstances.

Acknowledgments

We would like to thank A. Denig for discussions of the experimental aspects of our analysis.

Appendix A: g_1 and g_2 couplings

The effective couplings g_1 and g_2 are defined in Section II through loop integrals. We split them into two parts. One coming from diagrams containing $\chi_{c_i}-\gamma-\gamma$ vertex and called $g_{i_{\gamma\gamma}}$ and diagrams containing $\chi_{c_i}-J/\psi-\gamma$ vertex called $g_{i_{J/\psi\gamma}}$. The constants g_1 and g_2 are sums of these two contributions $g_i = g_{i_{\gamma\gamma}} + g_{i_{J/\psi\gamma}}$.

The couplings read ($M = M_{\chi_{c_1}}$ in g_1; $M = M_{\chi_{c_2}}$ in g_2; $M_J \equiv M_{J/\psi}$ in both); $x \equiv 4m^2/M^2$, $y \equiv 4M_{J/\psi}^2/M^2$

$$
\begin{aligned}
g_{1_{\gamma\gamma}} &= \frac{16\alpha^2 a}{\sqrt{m}M^2}\left[\log\left(\frac{x}{1+x}\right)(1-x)\right. \\
&\left.-\left(\log\left(\frac{x}{1-x}\right)+i\pi\right)(1+x)\right], \qquad \text{(A1)}
\end{aligned}
$$

$$
\begin{aligned}
g_{2_{\gamma\gamma}} &= \frac{32\sqrt{2}\alpha^2 a}{3\sqrt{m}M^2}\left[\left(\frac{1+x}{2}+\frac{8}{(1+x)^2}\right)\log(1-x)\right. \\
&+\frac{3}{2}(1+x)\log(1+x) - 2\left(1+x+\frac{2}{(1+x)^2}\right)\log(x) \\
&\left.-\frac{8}{(1+x)^2}\log(2) - 1 - \frac{i\pi}{2}\left(1+x+\frac{8}{(1+x)^2}\right)\right] \qquad \text{(A2)}
\end{aligned}
$$

$$
\begin{aligned}
g_{1_{J/\psi\gamma}} &= \frac{8\alpha^2 a_J f}{\sqrt{4\pi\alpha m}M^2M_J^2}\left[\left(\log\left(\frac{x}{1-x}\right)+i\pi\right)\left(1+x-\frac{y}{2}\right)\right. \\
&+F_0(x,y) - \frac{1}{4}(3+x+y)F_1(x,y) \\
&-\frac{y(4+y)}{2(2+2x-y)^2}F_2(x,y) + \frac{y(1+y-x)}{2(2+2x-y)}F_3(x,y) \\
&\left.-\frac{y}{2}F_4(x,y) + \frac{y}{2}(3-x)F_5(x,y)\right], \qquad \text{(A3)}
\end{aligned}
$$

$$
\begin{aligned}
g_{2_{J/\psi\gamma}} &= \frac{16\sqrt{2}\alpha^2 a_J f}{3\sqrt{4\pi\alpha m}M^2M_J^2}\left[2-\log(2)\left(3-\frac{16}{(1+x)^2}\right)\right. \\
&+\log(x)\left(1-y+2x+\frac{8}{(1+x)^2}\right) \\
&+\log(1-x)\left(\frac{1}{2}+y-2x-\frac{16}{(1+x)^2}\right) \\
&-\frac{3y}{8}\log\left(\frac{y}{4}\right)+\log\left(1-\frac{y}{4}\right)\left(-\frac{3}{2}+\frac{3y}{8}\right) \\
&\left.+i\pi\left(1-\frac{11y}{8}+2x+\frac{8}{(1+x)^2}\right)\right.
\end{aligned}
$$

$$
\begin{aligned}
&-F_0(x,y) - \left(\frac{1}{2}+y-\frac{x}{4}\right)F_1(x,y) \\
&+\frac{-55-123xy+126x+93x^2-94y+38y^2}{16(2+2x-y)^2}F_2(x,y) \\
&+\frac{87-5xy-2y+2y^2+2x+3x^2}{2(2+2x-y)}F_3(x,y) \\
&\left.-\frac{3y}{4}F_4(x,y) - \frac{3y}{4}(1+x)F_5(x,y)\right] \qquad \text{(A4)}
\end{aligned}
$$

with

$$
r = \sqrt{x-(1-y+x)^2/4} \qquad \text{(A5)}
$$

and

$$
\begin{aligned}
A(x,y) &= \arctan\left(\frac{1-y+x}{2r}\right) - \arctan\left(\frac{-1-y+x}{2r}\right) \\
F_0(x,y) &= \frac{1+y-x}{4}\log(x/y) - rA(x,y) \\
F_1(x,y) &= \log(x/y) + \frac{1+y-x}{r}A(x,y) \\
F_2(x,y) &= 2\log(2) - x\log(x) + y/2\log(y/2) \\
&-(1-x)(\log(1-x)-i\pi) \\
&+(2-y/2)(\log(2-y/2)-i\pi) \\
&+\frac{-1-x+y}{2}\log(x) + \frac{-1+x-y}{2}\log(y) \\
&-2rA(x,y) \\
F_3(x,y) &= -\frac{3}{2}\log(x) + \log(1-x) - i\pi \\
&+\frac{1}{2}\log(y) - \frac{1-x+y}{2r}A(x,y) \\
F_4(x,y) &= \log(1-2/y)\log(y/2) - \mathrm{Li}_2(2/y) \\
&+\mathrm{Li}_2\left(\frac{1-y/2}{1+x-y/2}\right) - \mathrm{Li}_2\left(\frac{-y/2}{1+x-y/2}\right) \\
&-\mathrm{Li}_2\left(\frac{1-y/2}{(1-x)/2+ir_1}\right) - \mathrm{Li}_2\left(\frac{1-y/2}{(1-x)/2-ir_1}\right) \\
&+\mathrm{Li}_2\left(\frac{-y/2}{(1-x)/2+ir_1}\right) + \mathrm{Li}_2\left(\frac{-y/2}{(1-x)/2-ir_1}\right) \\
F_5(x,y) &= -\frac{1}{1+x-y/2}\log\left(\frac{1+x}{x}\right) \\
&+\frac{-r_1+i(1+y-x)/2}{(1-x+2ir_1)r_1}\log\left(\frac{(1-x+y)/2+ir_1}{(-1-x+y)/2+ir_1}\right) \\
&-\frac{r_1+i(1+y-x)/2}{(1-x-2ir_1)r_1}\log\left(\frac{(1-x+y)/2-ir_1}{(-1-x+y)/2-ir_1}\right)
\end{aligned} \qquad \text{(A6)}
$$

with

$$
r_1 = \sqrt{x-(1+y-x)^2/4} \qquad \text{(A7)}
$$

[1] J. Kaplan and J. H. Kühn, Phys. Lett. **B78**, 252 (1978).
[2] J. H. Kühn, J. Kaplan, and E. G. O. Safiani, Nucl.Phys. **B157**, 125 (1979).
[3] N. Kivel and M. Vanderhaeghen, JHEP **02**, 032 (2016), 1509.07375.
[4] A. Denig, F.-K. Guo, C. Hanhart, and A. V. Nefediev, Phys. Lett. **B736**, 221 (2014), 1405.3404.
[5] D. Yang and S. Zhao, Eur. Phys. J. **C72**, 1996 (2012), 1203.3389.
[6] W. Buchmüller and S. Cooper, Adv. Ser. Direct. High Energy Phys. **1**, 410 (1988).
[7] K. Olive et al. (Particle Data Group), Chin.Phys. **C38**, 090001 (2014).
[8] H. Czyz, A. Grzelinska, and J. H. Kühn, Phys.Rev. **D81**, 094014 (2010), 1002.0279.
[9] H. Czyz and J. H. Kühn, Phys.Rev. **D80**, 034035 (2009), 0904.0515.
[10] G. Rodrigo, H. Czyz, J. H. Kühn, and M. Szopa, Eur.Phys.J. **C24**, 71 (2002), hep-ph/0112184.

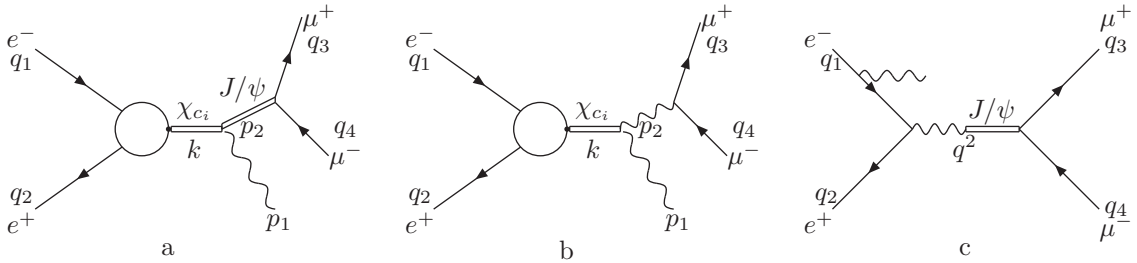
e^-
q_1
q_2
e^+
χ_{c_i}
k
J/ψ
p_2
p_1
μ^+
q_3
q_4
μ^-
a
e^-
q_1
q_2
e^+
χ_{c_i}
k
p_2
p_1
μ^+
q_3
q_4
μ^-
b
e^-
q_1
q_2
e^+
J/ψ
q^2
μ^+
q_3
q_4
μ^-
c